

Article

Bleached Wood Supports for Floatable, Recyclable, and Efficient Three Dimensional Photocatalyst

Yuming He ¹, Huayang Li ¹, Xuelian Guo ² and Rongbo Zheng ^{1,*}

¹ Yunnan Province Key Laboratory of Wood Adhesives and Glued Products, College of Chemical Engineering, Southwest Forestry University, Kunming 650224, China; hymingin@163.com (Y.H.); Li876770996@outlook.com (H.L.)

² Wetland college, Southwest Forestry University, Kunming 650224, China; guoxuelian2009@hotmail.com

* Correspondence: zhengrbzy@hotmail.com

Received: 21 December 2018; Accepted: 18 January 2019; Published: 26 January 2019



Abstract: To suppress the agglomeration of a photocatalyst, facilitate its recovery, and avoid photolysis of dyes, various support materials such as ceramic, carbon, and polymer have been investigated. However, these support materials pose the following additional challenges: ceramic supports will settle down at the bottom of their container due to their high density, while the carbon support will absorb the UV-vis light for its black color. Herein, we propose a floatable, UV transmitting, mesoporous bleached wood with most lignin removal to support P25 nanoparticles (BP-wood) that can effectively, recyclable, three dimensional (3D) photocatalytic degrade dyes such as methylene blue (MB) under ambient sunlight. The BP-wood has the following advantages: (1) The delignification makes the BP-wood more porous to not only quickly transport MB solutions upstream to the top surface, but is also decorated with P25 nanoparticles on the cell wall to form a 3D photocatalyst. (2) The delignification endows the BP-wood with good UV transmittance to undergo 3D photocatalytic degradation under sunlight. (3) It can float on the surface of the MB solution to capture more sunlight to enhance the photodegradation efficiency by suppressing the photolysis of MB. (4) It has comparable or even better photocatalytic degradation of 40 mg/L and 60 mg/L MB than that of P25 nanoparticles suspension. (5) It is green, recyclable, and scalable.

Keywords: bleached wood support materials; 3D photocatalyst; UV transmittance; floatable; recyclable

1. Introduction

In order to rapidly, efficiently, and cost-effectively remove dyes from industrial waste water [1], various technologies, such as physical adsorption [2], photocatalytic degradation, chemical oxidation, and membrane filtration, have been implemented, among which photocatalytic degradation has been demonstrated to be of high efficiency [3–5]. Heterogeneous photocatalysis is based on the use of UV light with a wavelength shorter than 380 nm to stimulate a semiconductor material (i.e., TiO₂ with band gap of ca. 3.2 eV, corresponding to radiation of UV light with a wavelength of about 380 nm) to excite the electrons from the valence band to the conduction band to generate electron–hole pairs, which serve as the oxidizing and reducing agents to photocatalytic degrade dyes [6]. The efficiency of TiO₂ was reported to be influenced by many factors, such as crystalline structure [7–10], particle size [10–13], and doping with the other ions [14–17]. However, there are some disadvantages in the use of TiO₂ nanoparticle suspension during photocatalytic processes: it tends to agglomerate at high concentrations, and is difficult to separate and recycle from the solution [18,19]. To overcome these disadvantages, TiO₂ can be supported on a material that suppresses the agglomeration and facilitates its further recovery. In this context, various support materials, such as ceramic (i.e., molecular

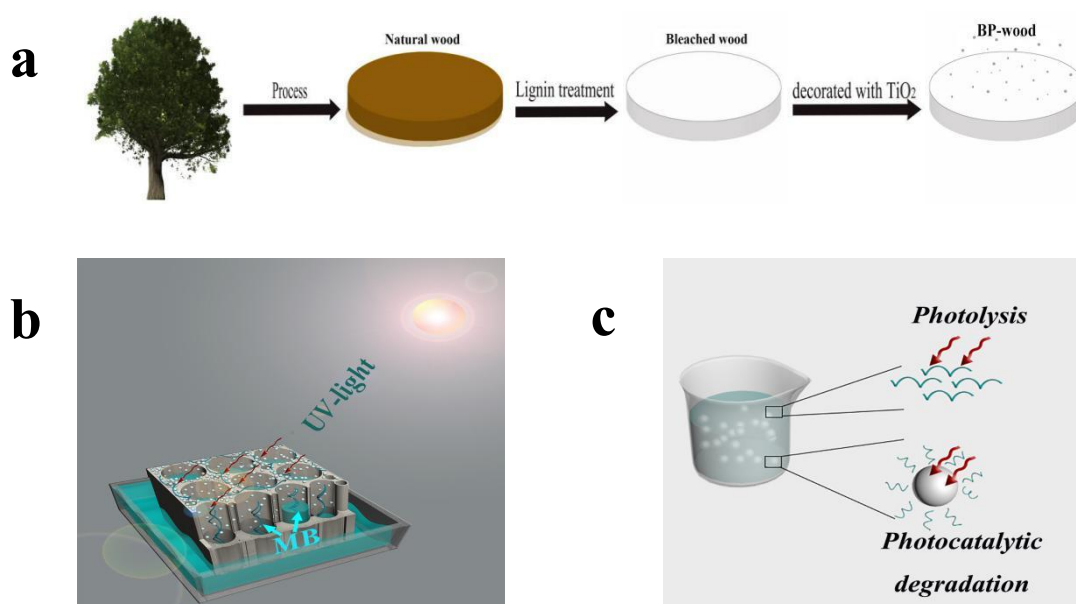
sieves, silica, zeolite, and clay) [19–22], carbon (i.e., activated carbon, carbon nanotube, graphene, and graphite) [18,23–26], and polymer (i.e., chitosan, polyamide, polyester) [27–29] have been investigated. However, these support materials pose additional challenges. For instance, ceramic supports will settle down at the bottom of their container due to their high density, while the dyes in the upper solution will absorb the UV light to have photolysis instead of photocatalytic degradation by the photocatalyst. The carbon support will absorb the UV-vis light due to its black color [30–32]. Thus, it is still a challenge to provide an excellent support material with low density to float on the dye solutions' surface to efficiently exploit UV light, 3D porous structure to support photocatalysts nanoparticles, transmit UV light and transport dye upstream.

Wood, an earth-abundant, natural, low density, hierarchical, mesoporous material, has been widely used as the template to prepare TiO₂ nanomaterials [33,34], the substrate to coat with TiO₂ nanoparticle to enhance weathering performance [35], and the support to decorate with palladium nanoparticles for efficient wastewater treatment [36]. With its mesoporous structure, wood is comprised of numerous long, partially aligned lumens as well as nanochannels along its growth direction, facilitating its floatation on the solutions' surface, decoration nanoparticles on the cell wall, and bulk treatment as water flows through the entire mesoporous wood [36]. However, it is difficult to exploit wood as a photocatalyst support due to the 20–30% lignin, whose absorption ranges from 300 nm to 600 nm [31].

The objective of the current study is to test the hypothesis that the bleached wood (i.e., cellulose-based hierarchical porous structure of wood obtained via delignification) can also be exploited as an alternative photocatalyst support material. Herein, P25, a commercial TiO₂ photocatalyst was coated on three kinds of wood-based supports, namely bleached wood with P25 (BP-wood), half-bleached wood with P25 (HBP-wood), and natural wood (N-wood) with P25 (NP-wood). The first two are obtained by removing about 50% lignin and 95% lignin, respectively. Notably, the mesoporous structure of N-wood is well maintained even after removing 95% lignin, and possess transmittance with UV light. The photocatalytic activity of above three wood-based catalysts are investigated in aqueous solution by using methylene blue (MB) dye as a model contaminant under ambient sunlight illumination. The mesoporous structure of the bleached wood is demonstrated to play important roles in the photocatalytic degradation since the wood is composed of 50% vessel channels and 20% fiber channels, which provide a pathway to quickly transport MB solution onto the top surface to be photodegraded with the P25 nanoparticles under sunlight illumination. Moreover, the P25 nanoparticles can be penetrated into the wood cell wall to form 3D photocatalytic composites to further enhance the photodegradation with the illumination of transmitted UV light. The experimental result shows that it has better photocatalytic degradation of 60 mg/L MB than that of P25 nanoparticles suspension.

2. Results and Discussion

Scheme 1a illustrates the preparation process of BP-wood and the photocatalytic process. In order to remove lignin, the natural basswood is delignified by H₂O₂ steam. Scheme 1b demonstrates the approximate photodegradation mechanism of BP-wood-supported catalysts. The degraded materials are continuously transported from the bottom of the BP-wood to the top and inside, forming a 3D catalytic mechanism under the permeation of the light source. As for the control group (P25 nanoparticles are directly added to the MB solution), shown in Scheme 1c. P25 is easily wrapped with the light-absorbing dye in the solution, so that the dye undergoes weak photolysis under illumination, which has a certain degree of influence on the photocatalytic degradation of P25.



Scheme 1. Material preparation and usage. (a) Sketch of BP-wood preparation. (b) Wood absorbs methylene blue (MB) from the bottom of the contact surface and sends MB to the location of lower concentration by capillary action and transpiration of the pipeline. With the provision of ultraviolet light from sunlight, TiO₂, once exposed to MB, immediately produces an effective photocatalytic degradation. There is also a degradation process of MB inside the timber pipe and inside the pipe wall. Due to the higher transmission of UV light in BP-wood, the P25 penetrating into the interior of the wood also plays a role of catalyzer. (c) Schematic diagram of a control group-added P25 particles directly.

The lignin content can be decreased from 22.5% (N-wood) to 12.3% (Half B-wood), to 1.01% (B-wood) when the H₂O₂ steam time prolong to 1 h and 4 h, respectively (shown in Figure 1a). The mechanical strength of BP-wood is shown in Figure 1b. For the wet BP-wood with a thickness of 5 mm, the fracture strength is about 0.4 MPa. It is lower than that of N-wood and dry BP-wood (2.4 MPa), which was strong enough to be carried out in the photocatalytic process. From Figure 1c,d, we can see that massive microscale pores were generated in the cell wall and cell wall corners after delignification compared with N-wood, which will provide sites to P25 nanoparticles, and a pathway to quickly transport dye solution upstream to the B-wood's top surface. Furthermore, P25 nanoparticles dispersed in aqueous solutions were coated on the surface of N-wood, Half B-wood, and B-wood to obtain P25 nanoparticles supported on the N-wood (NP-wood), Half B-wood (HBP-wood), and B-wood (BP-wood), respectively. As shown in Figure 1e, Raman spectra revealed that peak intensity of B-wood at 1300, 1602, and 1730 cm⁻¹ decreased compared with that of N-wood, which further demonstrated the removal of most of the lignin in B-wood [37]. Moreover, the degradation of the cellulose was negligible, while both lignin and hemicellulose were dramatically removed, as shown in our previous work [38]. The color changed from yellow to white during delignification process, shown in Figure 1f.

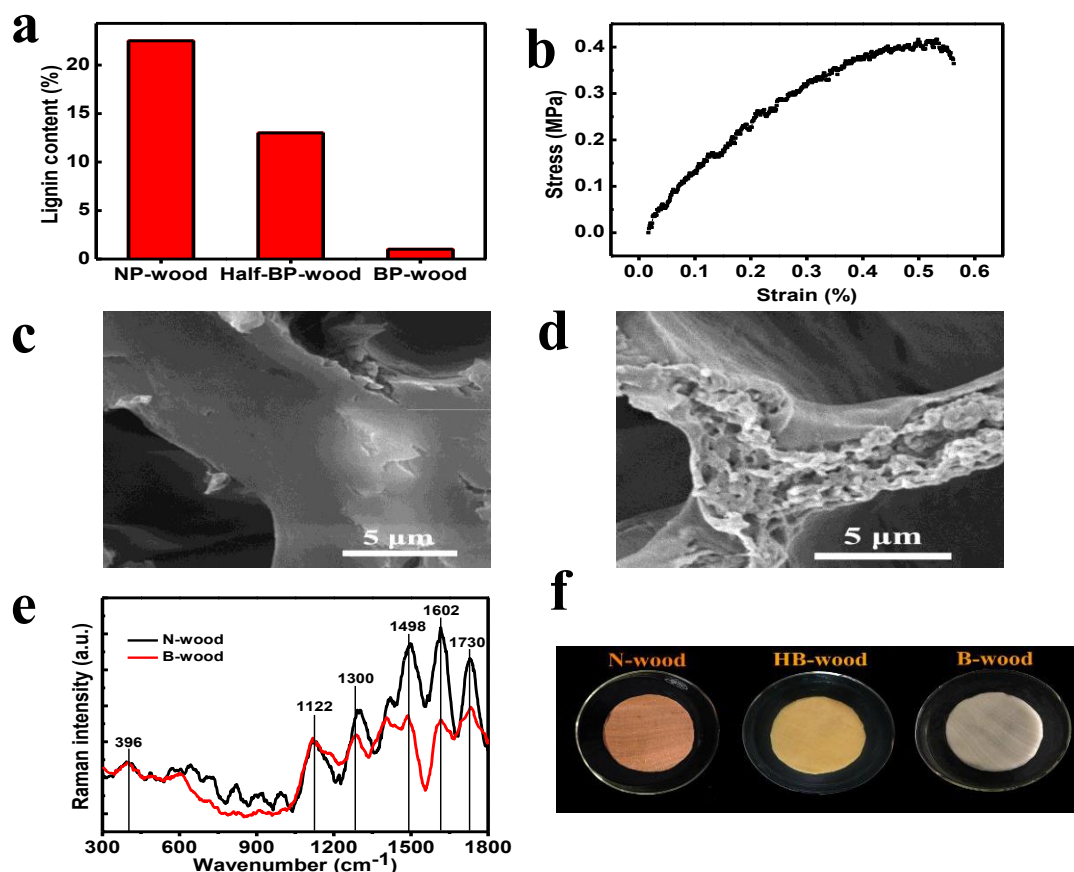


Figure 1. (a) Lignin content and (b) Mechanical strength of BP-wood in wet state. SEM images of cell wall corners and the middle lamella of (c) Natural basswood (N-wood) and (d) B-wood. (e) Raman characterization of N-wood, B-wood. The images were obtained through baseline corrected and normalized. (f) Photos of wood after removal of different content of lignin.

In order to investigate the water transportation capacity, we designed a dye transportation experiment. N-wood and B-wood are put into a dye solution to observe the distance the dye arrives after a certain time. As shown in Figure 2a, the dye in the B-wood reaches to a larger distance than that of the N-wood, which indicates that the B-wood exhibits better material transportation capabilities than that of N-wood. The speed of dye transportation in the B-wood and the N-wood are determined to be 2.2 and 6.3 mm/min, respectively (Figure 2b).

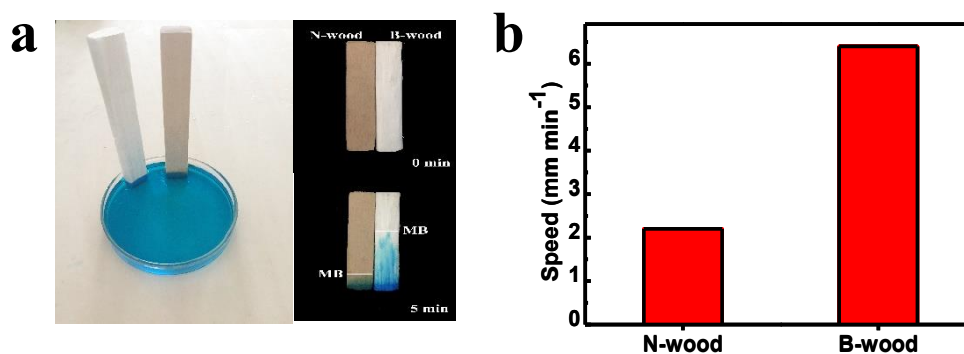


Figure 2. (a) The MB transport distance through B-wood and N-wood after 0, 5 min. (b) The MB transport speed through B-wood and N-wood during 5 min.

As shown in Figure 3a–d, P25 nanoparticles are not only decorated on the top surface of B-wood, but also penetrate into the cell wall of B-wood due to its mesoporous structure, which results in

three-dimensional (3D) P25-wood composites. The light transmittance of wet BP-wood and NP-wood in the range of 200–800 nm are shown in Figure 3e. It is worth noting that, in the ultraviolet range of 300–400 nm, BP-wood still has a light transmittance of 0.5–20%, while NP-wood does not have light transmittance before about 550 nm due to the existence of 22.5% lignin.

To demonstrate the 3D photocatalytic features of BP-wood, the P25 nanoparticles coated on the B-wood surface were purposely removed to preserve the P25 nanoparticles which had penetrated into the interior of the B-wood (BI-wood). 10 mg/L methylene blue (MB) aqueous solution was photocatalytically degraded with BI-wood, and B-wood under ambient sunlight. The re-plotted linear graph of $\ln(C_0/C) \sim t$ shown in Figure 3f indicates that the photocatalytic degradation of MB with P25 decorated inside the BP-wood follows roughly the pseudo-first-order reaction [7]. The rate constants were determined to be 0.35, 0.21, and 0.18 h^{-1} for BI-wood, B-wood, and methylene blue (MB) aqueous solution, respectively. That is, the photocatalytic degradation of BI-wood is better than absorption of B-wood and the photolysis of MB, which indicates that the bleached, delignified wood can be used as 3D photocatalyst support due to its mesoporous structure, and UV transmittance.

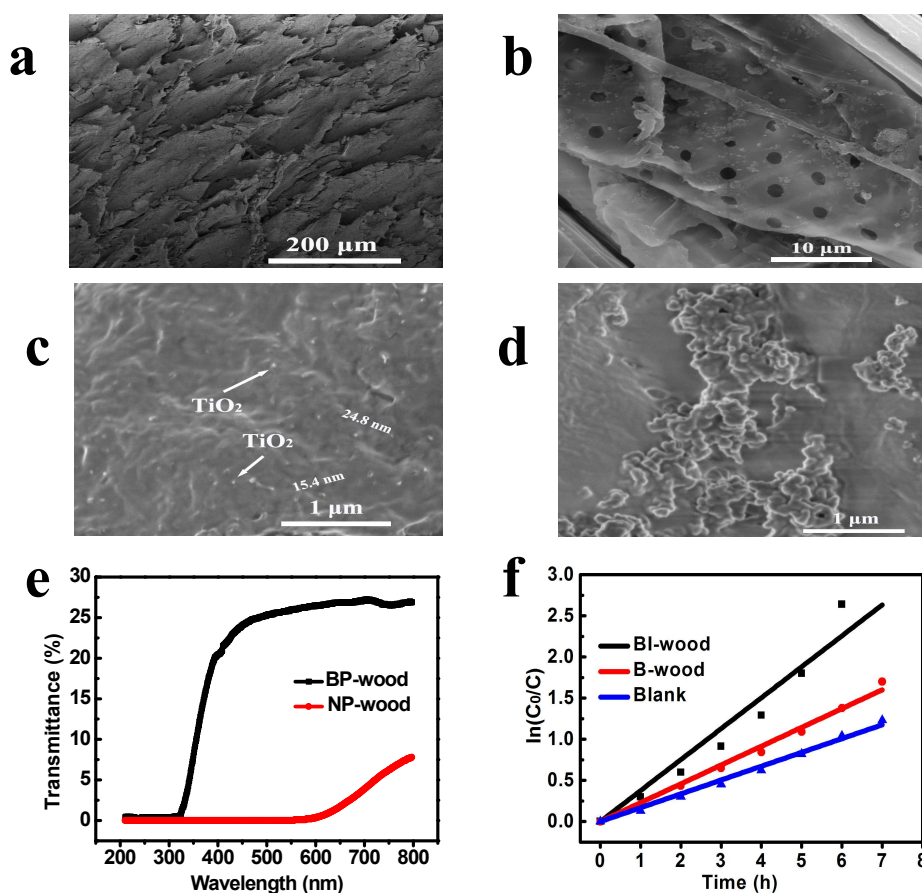


Figure 3. SEM images of B-wood's (a) top surface and (b–d) cross section decorated with P25 nanoparticles. (e) Optical transmittance of BP-wood and NP-wood. (f) Comparison of photocatalytic degradation of BI-wood with TiO_2 removed at the top and B-wood and blank control groups (where C_0 is the initial concentration of the dye solution and C is the concentration of dye at corresponding time) [6].

The photocatalytic properties of BP-wood, HBP-wood, and NP-wood were examined by measuring the photodegradation of 20 mg/L MB under ambient sunlight. As shown in Figure 4a, all wood-based photocatalysts, including BP-wood, HBP-wood, and NP-wood can float on the surface of the MB solution, and the P25 nanoparticles coating the top surface of the BP-wood are directly exposed to sunlight. Figure 4b shows the MB photolysis and photodegradation kinetic curves for reactions in

which P25, NP-wood, HBP-wood, and BP-wood are used as photocatalysts. Overall, the photocatalytic activity increased when the lignin content decreasing. The re-plotted linear graph of $\ln(c_0/c) \sim t$ shown in Figure 4b indicates that the rate constants were determined to be 0.52, 0.41, 0.21, and 0.08 h^{-1} for P25, BP-wood, HBP-wood, and NP-wood, respectively. Combining with the corresponding lignin content, we can conclude that the photocatalytic activity of wood supported P25 increases with the decreasing of lignin content. Notably, the photolysis of MB with 20 mg/L is very small. After photodegradation, both BP-wood and NP-wood were taken out from the solutions. It is clear that, after the photodegradation, the P25 nanoparticles' suspension leads to a turbidity inside the entire beaker, which indicates the difficulty to be separated and recycled (Figure 4c). As for NP-wood, the solution after photodegradation exhibits yellow color due to the leaching of N-wood [32]. However, it is clean and pollution-free for BP-wood, which reveals the clean and environmental benign. We further exam the BP-wood and NP-wood after photodegradation, shown in Figure 4d,e. Compared with the blue color of the interior of NP-wood, BP-wood appears pure white without MB molecules. That is, the MB molecules inside BP-wood are also photocatalytical degraded, which further demonstrates the 3D photocatalyst feature of BP-wood. As for NP-wood, although there was photocatalytic degradation occurring on the surface, the MB molecules absorbed in the porous wood still remained.

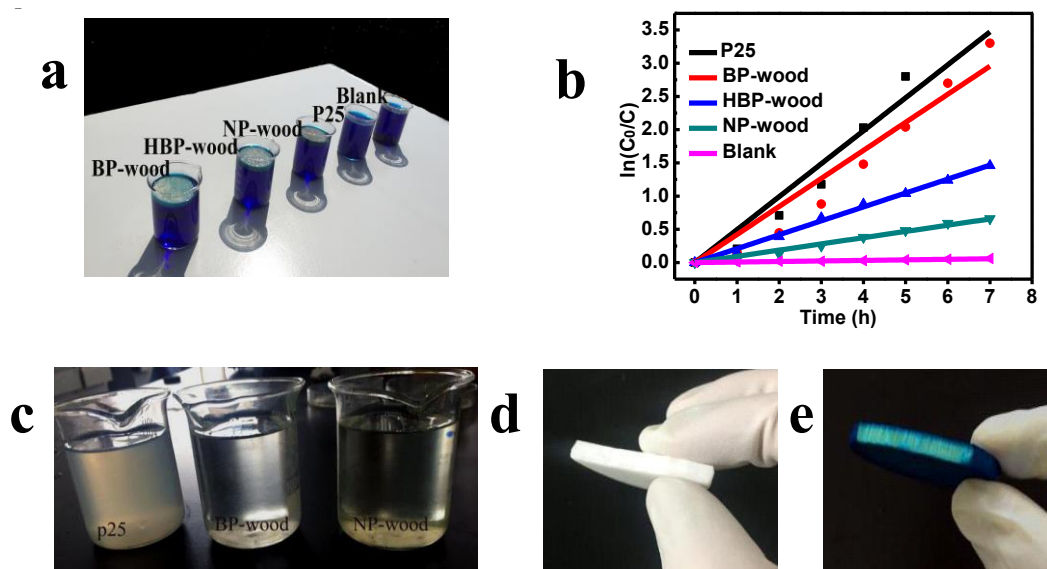


Figure 4. (a) Photo of photocatalytic degradation devices under sunlight. (b) Photodegradation of MB monitored as the normalized concentration change versus irradiation time under sunlight. Photo of (c) MB solutions, (d) BP-wood, and (e) NP-wood after photodegradation of MB solution under sunlight.

We also characterize the photocatalytic degradation of the high-concentration MB solution with BP-wood under ambient sunlight. From Figure 5a,b, we can see that the photodegradation performance of the BP-wood is comparable to or even better than those of P25 suspension when the concentration of MB increases to 40 mg/L and 60 mg/L, respectively. As we know, MB molecules can be degraded by either photolysis or photocatalytic degradation. With the MB concentration increased, MB molecules will absorb more UV light to be degraded by photolysis, which decreases the photocatalytic degradation efficiency of P25 suspension, while the effect on BP-wood is negligible due to its floatability. Figure 5c further demonstrates that the enhancement factor of the BP-wood versus P25 suspension increased with the increasing of MB concentration.

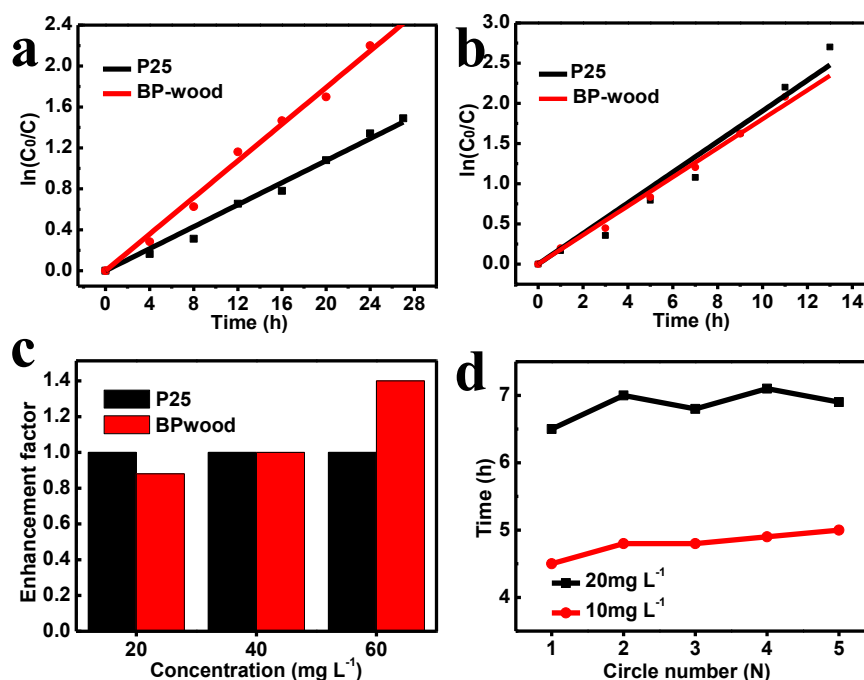


Figure 5. Photodegradation of MB solutions with (a) 40 mg/L, (b) 60 mg/L monitored as the normalized concentration change versus irradiation time in the presence of P25 and BP-wood under ambient sunlight. (c) Enhancement factor of the use of BP-wood compared with P25. (d) Recycling performance of BP-wood.

The photodegradation process of BP-wood consists of the following steps. Firstly, the BP-wood floats on the surface of MB aqueous solutions due to its low density. Secondly, the MB solutions will transport to the top surface of the BP-wood via aligned channels to make contact with P25 nanoparticles. Thirdly, MB molecules will be photocatalytically degraded via P25 nanoparticles under UV light with a wavelength shorter than 380 nm in sunlight. Fourth, MB molecules will continuously accumulate in both top surface and the interior of BP-wood via a concentration gradient to continuous photodegradation. It should be noted that the P25 nanoparticles decorated into the cell wall of BP-wood also exhibit photocatalytic activity since UV light can be transmitted into the interior of BP-wood.

Thanks to its large size and 0.4 MPa mechanical strength, BP-wood can be easily recycled to photodegrade the MB solution under ambient sunlight. After the degradation, the BP-wood was taken out and kept under ambient conditions. As shown in Figure 5d, our BP-wood exhibited excellent recyclable performance: during the 5 circles, it takes 6.5, 7.0, 6.8, 7.1, and 6.9 h respectively to achieve photodegradation of a 20 mg/L MB solution. There is no significant decline in efficiency during the photodegradation process.

3. Materials and Methods

3.1. Materials and Chemicals

Basswood was used in this study. P25 was bought from Degussa AG. H₂O₂, MB, anhydrous ethanol were bought from Sigma Chemicals (Shanghai, China).

3.2. Preparation of N-Wood and B-Wood

Natural basswood (N-wood) slices with size of $\pi \times 20 \times 20 \times 5$ mm³ were obtained by cutting along the direction perpendicular to the growth of wood. Half-B-wood and B-wood were obtained by H₂O₂ steam delignification of above-mentioned N-wood at 100 °C for 1 and 4 h, respectively [38]. After rinsed with water, and ethanol for three times, they were dried at 50 °C for 4 h.

3.3. Preparation of NP-Wood and BP-Wood

The P25 nanoparticles were dispersed in deionized water and ultrasonically dispersed for 10 min. After overnight, the upper 5 mL * 3 g/L P25 suspension was coated on the N-wood, Half-B-wood, and B-wood to form NP-wood, HBP-wood, and BP-wood.

3.4. Photocatalytic Activity Measurement

The photocatalytic activity of the aforementioned samples was investigated by placing NP-wood, HBP-wood, and BP-wood on the surface of MB aqueous solution to measure the P25-assisted photodegradation of 100 mL MB aqueous solutions. At the same time, 0 mL and 5 mL * 3 g/L P25 suspension was added into 100 mL MB aqueous solutions as the control group. Then, they were irradiated under ambient sunlight. Finally, the concentration of MB after illuminating for a certain time was monitored by measuring the absorbance of the solutions (which were centrifuged at 2000 rpm to remove P25) at 664 nm.

3.5. Characterization

Scanning electron microscopy images were determined with a Nova NanoSEM 450, Lincoln, Ne, USA. The accelerating voltage was 15 kV. The UV-vis absorption was measured on Cary 500 Scan UV-vis-NIR spectrophotometer (Harbor, CA, USA). The transmittance of the material comes from the ultraviolet visible spectrophotometer. The UV-visible spectrophotometer model is U-4100 Spectrophotometer, Hitachi (Tokyo, Japan). A universal mechanical test machine was used to measure the mechanical properties with the SUNS UTM-5000 electronic universal testing machine (Shenzhen, China). The size of the test sample was $10 \times 1 \times 0.5 \text{ cm}^3$. And Raman spectra were obtained from LabRam HR Evolution, Horiba, France.

4. Conclusions

To summarize, a floatable, recyclable, efficient, UV light permeable, environmentally friendly, and 3D photocatalyst was easily synthesized through decoration with P25 nanoparticles on both the surface and in the interior of bleached wood. The bleached wood was obtained by removing most lignin from N-wood through H_2O_2 steam delignification. The delignification not only endows bleached wood with UV light transmittance, but also provides a highway to transport the MB solution up to the top surface. The as-made BP-wood photocatalyst shows a high photocatalytic degradation of 60 mg/L MB solution under ambient sunlight, better than that of P25 nanoparticles suspension. It also exhibits excellent recyclability due to its large size, floatability, and 0.4 MPa mechanical strength. The present work opens up an efficacious avenue for designing bleached wood-based recyclable, floatable, UV permeable, and efficient 3D photocatalyst for environmental pollution.

Author Contributions: Conceptualization, R.Z. and Y.H.; methodology, Y.H.; software, R.Z.; validation, R.Z. and X.G.; formal analysis, H.L.; investigation, X.G.; resources, R.Z.; data curation, R.Z.; writing—original draft preparation, Y.H.; writing—review and editing, R.Z.; visualization, R.Z.; supervision, R.Z.; project administration, R.Z. and X.G.; funding acquisition, R.Z. and X.G.

Funding: This research was funded by the Joint Special Project of Agricultural Basic Research in Yunnan (2017FG001036). And the APC was funded by the National Natural Science Foundation of China, grant number 41563008, 31100420.

Conflicts of Interest: The authors declare no conflict of interest.

References

1. Ren, Z.J.; Umble, A.K. Water treatment: Recover wastewater resources locally. *Nature* **2016**, *529*, 25. [[CrossRef](#)] [[PubMed](#)]
2. Maity, S.K.; Rana, M.S.; Bej, S.K.; Ancheyta-Juárez, J.; Murali Dhar, G.; Prasada Rao, T.S.R. TiO_2 - ZrO_2 mixed oxide as a support for hydrotreating catalyst. *Catal. Lett.* **2001**, *72*, 115–119. [[CrossRef](#)]

3. Ali, I. New generation adsorbents for water treatment. *Chem. Rev.* **2012**, *112*, 5073–5091. [[CrossRef](#)] [[PubMed](#)]
4. Panizza, M.; Cerisola, G. Direct and mediated anodic oxidation of organic pollutants. *Chem. Rev.* **2009**, *109*, 6541–6569. [[CrossRef](#)] [[PubMed](#)]
5. Huang, L.; Chen, J.; Gao, T.; Zhang, M.; Li, Y.; Dai, L.; Qu, L.; Shi, G. Reduced graphene oxide membranes for ultrafast organic solvent nanofiltration. *Adv. Mater.* **2016**, *28*, 8669–8674. [[CrossRef](#)] [[PubMed](#)]
6. Gratzel, M. *Photocatalysis: Fundamentals and Applications*; Serpone, N., Pelizzetti, E., Eds.; Wiley: New York, NY, USA, 1989; p. 123.
7. Zheng, R.B.; Meng, X.W.; Tang, F.Q. Synthesis, characterization and photodegradation study of mixed-phase titania hollow microspheres with rough surface. *Appl. Surf. Sci.* **2009**, *255*, 5989–5994. [[CrossRef](#)]
8. Nishimoto, S.I.; Ohtani, B.; Kajiura, H.; Kagiya, T. ChemInform abstract: Correlation of the crystal structure of titanium dioxide prepared from titanium tetra-2-propoxide with the photocatalytic activity for redox reactions in aqueous propan-2-ol and silver salt solutions. *J. Chem. Soc. Faraday Trans.* **1985**, *16*, 61–68. [[CrossRef](#)]
9. Fox, M.A.; Dulay, M.T. Heterogeneous photocatalysis. *Chem. Rev.* **1993**, *93*, 341–357. [[CrossRef](#)]
10. Tanaka, K.; Hisanaga, T.; Rivera, A.P. *Photocatalytic Purification and Treatment of Water and Air*; Ollis, D.F., Al-Ekabi, H., Eds.; Elsevier: Amsterdam, The Netherlands, 1993; p. 169.
11. Yoneyama, H.; Yamanaka, S.; Haga, S. Photocatalytic activities of microcrystalline titania incorporated in sheet silicates of clay. *J. Phys. Chem.* **1989**, *93*, 4833–4837. [[CrossRef](#)]
12. Zhang, Z.; Wang, C.C.; Zakaria, R.; Ying, J. Role of particle size in nanocrystalline TiO₂-based photocatalyst. *J. Phys. Chem. B* **1998**, *102*, 10871–10878. [[CrossRef](#)]
13. Tsai, S.-J.; Cheng, S. Effect of TiO₂ crystalline structure in photocatalytic degradation of phenolic contaminants. *Catal. Today* **1997**, *33*, 227–237. [[CrossRef](#)]
14. Paola, A.D.; Ikeda, S.; Marci, G.; Ohtani, B.; Palmisano, L. Photocatalytic degradation of organic compounds in aqueous systems by transition metal doped polycrystalline TiO₂. *Catal. Today* **2002**, *75*, 171–176. [[CrossRef](#)]
15. Hu, C.C.; Hsu, T.C.; Kao, L.H. One-step cohydrothermal synthesis of nitrogen-doped titanium oxide nanotubes with enhanced visible light photocatalytic activity. *Int. J. Photoenergy* **2012**, 391958. [[CrossRef](#)]
16. Chen, X.; Mao, S.S. Titanium dioxide nanomaterials synthesis, properties, modifications, and applications. *Chem. Rev.* **2007**, *107*, 2891–2959. [[CrossRef](#)] [[PubMed](#)]
17. Al Dahoudi, N.; Zhang, Q.; Cao, G. Alumina and hafnia ALD Layers for a niobium-doped titanium oxide photoanode. *Int. J. Photoenergy* **2012**, 401393. [[CrossRef](#)]
18. Zheng, R.B.; Meng, X.W.; Tang, F.Q. A general protocol to coat titania shell on carbon-based composite cores using carbon as coupling agent. *J. Solid State Chem.* **2009**, *182*, 1235–1240. [[CrossRef](#)]
19. Hsien, Y.H.; Chang, C.F.; Chen, Y.H.; Cheng, S. Photodegradation of aromatic pollutants in water over TiO₂ supported on molecular sieves. *Appl. Catal. B Environ.* **2001**, *31*, 241–249. [[CrossRef](#)]
20. Sampath, S.; Uchida, H.; Yoneyama, H. Photocatalytic degradation of gaseous pyridine over zeolite-supported titanium dioxide. *J. Catal.* **1994**, *149*, 189–194. [[CrossRef](#)]
21. Van Grieken, R.; Aguado, J.; López-Muñoz, M.J.; Marugán, J. Synthesis of size-controlled silica-supported TiO₂ photocatalysts. *J. Photochem. Photobiol. A Chem.* **2012**, *148*, 315–322. [[CrossRef](#)]
22. Paul, B.; Martens, W.N.; Frost, R.L. Immobilised anatase on clay mineral particles as a photocatalyst for herbicides degradation. *Appl. Clay Sci.* **2012**, *57*, 49–54. [[CrossRef](#)]
23. Baek, M.H.; Yoon, J.W.; Hong, J.S.; Suh, J.K. Application of TiO₂-containing mesoporous spherical activated carbon in a fluidized bed photoreactor—Adsorption and photocatalytic activity. *Appl. Catal. A Gen.* **2013**, *45*, 222–229. [[CrossRef](#)]
24. Chaturvedi, S.; Dave, P.N.; Shah, N.K. Applications of nano-catalyst in new era. *J. Saudi Chem. Soc.* **2016**, *16*, 307–325. [[CrossRef](#)]
25. Hsieh, S.H.; Chen, W.J.; Wu, C.T. Pt-TiO₂/Graphene photocatalysts for degradation of AO₇ dye under visible light. *Appl. Surf. Sci.* **2015**, *340*, 9–17. [[CrossRef](#)]
26. Li, D.; Jia, J.; Zhang, Y.; Wang, N.; Guo, X.; Yu, X. Preparation and characterization of Nano-graphite/TiO₂ composite photoelectrode for photoelectrocatalytic degradation of hazardous pollutant. *J. Hazard. Mater.* **2016**, *315*, 1–10. [[CrossRef](#)] [[PubMed](#)]
27. Hamdi, A.; Boufi, S.; Bouattour, S. Phthalocyanine/chitosan-TiO₂ photocatalysts: Characterization and photocatalytic activity. *Appl. Surf. Sci.* **2015**, *339*, 128–136. [[CrossRef](#)]

28. Lei, Y.; Zhang, C.; Lei, H.; Huo, J. Visible light photocatalytic activity of aromatic polyamide dendrimer/TiO₂ composites functionalized with spirolactam-based molecular switch. *J. Colloid Interface Sci.* **2013**, *406*, 178–185. [[CrossRef](#)]
29. Mejía, M.I.; Marín, J.M.; Restrepo, G.; Rios, L.A.; Pulgarín, C.; Kiwi, J. Preparation, testing and performance of a TiO₂/polyester photocatalyst for the degradation of gaseous methanol. *Appl. Catal. B* **2010**, *94*, 166–172. [[CrossRef](#)]
30. Zhu, M.W.; Li, Y.J.; Chen, G.; Jiang, F.; Yang, Z.; Luo, X.G.; Wang, Y.B.; Lacey, S.D.; Dai, J.Q.; Wang, C.W.; et al. Tree-inspired design for high-efficiency water extraction. *Adv. Mater.* **2017**, *29*, 1704107. [[CrossRef](#)]
31. Liu, H.; Chen, C.J.; Chen, G.; Kuang, Y.D.; Zhao, X.P.; Song, J.W.; Jia, C.; Xu, X.; Hitz, E.; Xie, H.; et al. High-performance solar steam device with layered channels: Artificial tree with a reversed design. *Adv. Energy Mater.* **2017**, *8*, 1701616. [[CrossRef](#)]
32. Chen, C.; Li, Y.; Song, J.; Yang, Z.; Kuang, Y.; Hitz, E.; Jia, C.; Gong, A.; Jiang, F.; Zhu, J.Y.; et al. Highly flexible and efficient solar steam generation device. *Adv. Mater.* **2017**, *29*, 1701756. [[CrossRef](#)]
33. Sun, Q.F.; Lu, Y.; Tu, J.C.; Li, J. Bulky macroporous TiO₂ photocatalyst with cellular structure via facile wood-template method. *Int. J. Photoenergy* **2013**, 649540. [[CrossRef](#)]
34. Gao, L.K.; Gan, W.T.; Li, J. Preparation of heterostructured WO₃/TiO₂ catalysts from wood fibers and its versatile photodegradation abilities. *Sci. Rep.* **2017**, *7*, 1102. [[CrossRef](#)] [[PubMed](#)]
35. Zheng, R.B.; Tshabalala, M.A.; Li, Q.Y.; Wang, H.Y. Construction of hydrophobic wood surfaces by room temperature deposition of rutile (TiO₂) nanostructures. *Appl. Surf. Sci.* **2015**, *28*, 453–458. [[CrossRef](#)]
36. Chen, F.J.; Gong, A.S.; Zhu, M.W.; Hu, L.B. Mesoporous, three-dimensional wood membrane decorated with nanoparticles for highly efficient water treatment. *ACS Nano* **2017**, *11*, 4275–4282. [[CrossRef](#)] [[PubMed](#)]
37. Jana, S.; Vanessa, S.; Tobias, K.; Ingo, B. Characterization of wood derived hierarchical cellulose scaffolds for multifunctional applications. *Materials* **2018**, *11*, 517. [[CrossRef](#)]
38. Li, H.Y.; Guo, X.L.; He, Y.M.; Zheng, R.B. A green, steam-modified delignification method to low lignin delignified wood for thick, large, highly transparent wood composites. *J. Mater. Res.* **2018**. [[CrossRef](#)]



© 2019 by the authors. Licensee MDPI, Basel, Switzerland. This article is an open access article distributed under the terms and conditions of the Creative Commons Attribution (CC BY) license (<http://creativecommons.org/licenses/by/4.0/>).